J Ther Eng, Vol. 9, No. 4, pp. 998−1014, July, 2023

Journal of Thermal Engineering
Web page info: https://jten.yildiz.edu.tr
DOI: 10.18186/thermal.000000

Journal of Thermal Engineering

Research Article

Analysis of heat transfer and flow over a rotating cylinder at subcritical Reynolds numbers based on Taguchi method

Ebrahim BARATI[1], Mehdi Rafati ZARKAK[1], Shohreh JALALI[1]

[1]*Department of Mechanical Engineering, Khayyam University, Mashhad, 9189747178, Iran*

ARTICLE INFO

Article history
Received: 09 October 2021
Revised: 16 March 2022
Accepted: 19 April 2022

Keywords:
Thermal Buoyancy; Rotational Cylinder; Vortex Shedding; Aerodynamic Force; Taguchi Method

ABSTRACT

The flow past the rotating circular cylinder and the effect of buoyancy on heat transfer characteristics are studied numerically for the Reynolds number of 20 and 40 and the Prandtl number of 0.7. The lift and drag coefficients, Strouhal number, and local Nusselt number on the cylinder are studied under the sway of combined buoyancy (at the Richardson number varies from 0 to 2) and different rotational directions. Although the interaction between buoyancy and rotation is a puzzling heat transfer problem, the direction of rotation is found to have significant effects on the flow patterns and heat transfer rate. The main innovation of the present work is to determine the extreme points of Nusselt numbers when different conditions are applied. For a positive rotation, the maximum local Nusselt number is at $\theta=225^{o}$, and the minimum local Nusselt number is at $\theta=100^{o}$. In contrast, for a negative rotation, the maximum and minimum local Nusselt numbers are at $\theta=140^{o}$ and $\theta=270^{o}$, respectively. Applying Taguchi method, it is found that average Nusselt number is more dependent on Reynolds number than other factors. Additionally, it can be concluded that the direction of rotation can be used as a powerful tool to adjust the heat transfer rate and the required value of drag and lift. Consequently, without applying different rotation speeds, it would be difficult to stabilize the flow, and with the aid of Taguchi method, it is determined that rotation is deciding factor in stabilizing flow patterns. The results are in good agreement with the experimental results.

Cite this article as: Barati E, Zarkak MR, Jalali S. Analysis of heat transfer and flow over a rotating cylinder at subcritical Reynolds numbers based on Taguchi method. J Ther Eng 2023;9(4):998−1014.

INTRODUCTION

When a flow passes over a bluff body, a vortex called Von Karman vortex shedding (VS) is generated. The fluid patterns and heat transfer behavior around the cylinder are affected by the VS behind this body. The buoyancy force and rotation alter the properties of the VS and play a key role in wake dynamics. The inclusion of the buoyancy force causes the VS excitation and the increase in the VS frequency as a function of the flow direction [1, 2]. The superimposed thermal buoyancy force induces oscillations in the velocity field, which causes periodic Nu changes on the surface of the bluff body and influences the lift and drag

*Corresponding author.
*E-mail address: ebrahim_barati@yahoo.com

This paper was recommended for publication in revised form by Editor in Chief N. Filiz Özdil

coefficients resulting from the separation of the boundary layer delay [3].

Paramane and Sharma [4] studied the buoyancy-induced generation of the VS around the rotating cylinder at Re of 40 and 100. They employed air as the working fluid, and the dimensionless rotational velocity was changed from 0 to 8 with different Ri. Al-Sumaily et al. [5] performed a numerical study to improve the understanding of the effect of thermal buoyancy on flow properties. They found that the larger Ri is, the larger the amplitude of the shedding; consequently, strong vortices are shed, leading to an increase in heat transfer rates. Chatterjee et al. [6] studied the effect of buoyancy on VS behind the rotating circular cylinder at subcritical Re. They chose a range of Re from 5 to 45, different speeds, and Ri from 0 to 2. Their results showed that the flow becomes transient when Ri is increased at a constant speed. They found that more heating is required to destabilize the flow patterns when the rotational speed increases.

In connection with the effect of mixed convection and rotation in bluff bodies, Nguyen et al. [7] studied mixed convection around a rotating circular cylinder. Re of 100 and 200, Gr of 20,000, and rotational velocity of -0.5 to +0.5 were considered. It was found that VS increases due to the rotation of the cylinder, but disappears when the buoyancy force is added. Elghnam [8] studied experimentally and numerically the effect of rotation on heat transfer from a heated horizontal cylinder rotating in still air around its axes. In this study, the air was considered stationary, and it was found that the dependence of Nu on Gr decreases as the value of Re increases, and it vanishes at higher values of Re. Luo et al. [9] performed a numerical simulation to study the flow characteristics and heat transfer process when a fluid flows past an oscillating cylinder. Their results show that the heat transfer improves significantly with amplitude and frequency increase. In their study, the field synergy principle was used to analyze the influence mechanism of the improved heat transfer. Wan et al. [10] conducted research whose leading innovation was to understand the mechanism of the interaction between buoyancy and rotation and its effects on VS, aerodynamic properties, and heat transfer rates of a heated cylinder with circular cross-section directly subjected to a cross flow. In addition, an elastic cylinder was used, and the alignment between the flow direction and thermally induced buoyancy force was applied. Mahir and Altaç [11] studied the effects of Reynolds, Richardson and Prandtl numbers on the flow field and temperature distributions. They found that the flow and heat transfer characteristics are influenced more for air than water.

The study of thermal fluid flow around a rotating cylinder is of great engineering importance for myriad applications, including rotary tubes, heat exchanger tubes, and rotary shafts [12-14]. The unsteady incompressible fluid over an accelerated moving vertical plate through a porous medium in a rotating system was studied by Hussain et al. [15], and they concluded that the rotation and chemical reaction tend to enhance primary skin friction. In addition, the study of flow around a cylinder is critical for cooling electronic devices and other engineering applications, including drying various things, glass cooling, plastics, and industrial equipment. In most published works, the influence of the direction of rotation associated with the buoyancy force has not been fully understood.

Against this background, a deep understanding of the mechanism of the fluid-structure interaction for a rotating cylinder is still lacking owing to the complexity of the interaction between a cylinder and wake region, from the literature survey for stationary cylinder, it is found that the cross-stream buoyancy destabilizes the flow. However, the impact of rotation direction on flow patterns is not fully understood when the flow velocity is not high enough to be dominant. Therefore, the aim of this work is to explore the influence of the rotation direction on flow and heat transfer. Moreover, with the help of Taguchi method, the importance of each factor compared with others is defined. This study sets out to numerically investigate the combined effect of the thermal buoyancy force and direction of rotation (clockwise and counterclockwise) at subcritical Re on heat transfer and fluid mechanics, employing Taguchi method to determine influential factors in heat transfer and flow patterns.

Description of the Physical Problem

For the present simulation, a Newtonian incompressible and laminar flow with fixed thermophysical properties is used together with the Boussinesq approximation. The governing equations in the dimensionless form are introduced as follows:

Continuity equation:

$$\frac{\partial u}{\partial x}+\frac{\partial v}{\partial y}=0 \tag{1}$$

x- and y-momentum equations:

$$\frac{\partial u}{\partial t}+u\left(\frac{\partial u}{\partial x}\right)+\mathrm{v}\left(\frac{\partial u}{\partial y}\right)=-\frac{\partial p}{\partial x}+\frac{1}{\mathrm{Re}}\left(\frac{\partial^2 u}{\partial x^2}+\frac{\partial^2 u}{\partial y^2}\right)+\mathrm{F}_{X'} \tag{2}$$

$$\frac{\partial v}{\partial t}+u\left(\frac{\partial v}{\partial x}\right)+\mathrm{v}\left(\frac{\partial u}{\partial y}\right)=-\frac{\partial p}{\partial y}+\frac{1}{\mathrm{Re}}\left(\frac{\partial^2 v}{\partial x^2}+\frac{\partial^2 v}{\partial y^2}\right)+Ri\theta+\mathrm{F}_{y'} \tag{3}$$

where F_x and F_y are external forces in x and y directions, respectively.

Thermal energy equation:

$$\frac{\partial \theta}{\partial t}+u\left(\frac{\partial \theta}{\partial x}\right)+\mathrm{v}\left(\frac{\partial \theta}{\partial y}\right)=\frac{1}{\mathrm{RePr}}\left(\frac{\partial^2 \theta}{\partial x^2}+\frac{\partial^2 \theta}{\partial y^2}\right) \tag{4}$$

These variables have been used to make the above equations dimensionless.

$$u=\frac{\bar{u}}{U_\infty}, v=\frac{\bar{v}}{U_\infty}, x=\frac{X}{D}, \mathrm{y}=\frac{Y}{D}, p=\frac{\bar{p}}{\rho U_\infty^2}, \mathrm{t}=\frac{\bar{t}U_\infty}{D}, \theta=\frac{T-T_\infty}{T_W-T_\infty} \quad (5)$$

Boundary conditions for the flow and temperature field are as follows:

The top and bottom boundaries of the domain:

$$\frac{\partial u}{\partial y}=v=0, \theta=0 \quad (6)$$

At the entrance of the domain, the flow condition is considered:

$$u=1, v=0, \theta=0 \quad (7)$$

At the exit of the domain, the boundary condition is used by setting:

$$\frac{\partial u}{\partial x}=0, v=0, \theta=0 \quad (8)$$

The boundary condition on the cylinder surface is considered:

$$u=v=0, \theta=1 \quad (9)$$

An average Nu for the cylinder is introduced as:

$$Nu=\frac{hD}{k}, h=\frac{1}{2\pi}\int_0^{2\pi} h_{loc}\, d\theta \quad (10)$$

The dimensionless rotational velocity of the cylinder and eddy length are defined as:

$$\Omega=\frac{\omega}{\frac{2U_\infty}{D}} \quad (11)$$

$$L_{sep}=\frac{L_s}{D} \quad (12)$$

St is the Strouhal number, which is the ratio between the velocity of the cylinder and the free stream, and Ri is the Richardson number, which is a combination of the Grashof number and the Reynolds number:

$$St=\frac{f_{vs}D}{U_\infty} \quad (13)$$

$$Ri=\frac{Gr}{\mathrm{Re}^2} \quad (14)$$

Numerical Method

A two-dimensional (2D) flow analysis is incorporated by implementing the Computational Fluid Dynamic (CFD) method and using the Fluent analysis system from ANSYS FLUENT 2020 software [16]. The conservation equations, subject to the above-mentioned boundary conditions, are solved using a finite-volume method based on the SIMPLEC algorithm. The discretization of the equations is performed using the second-order upwind differencing scheme. Finally, the convergence criteria for governing equations are assumed to be satisfied when the sum of the residuals is less than 10^{-5}.

Computational Domain

The computational domain is varied to achieve an appropriate size. According to Figure 1, the domain is finally chosen to take into account the accuracy of the results and the convenience of modeling. The length of the computational domains is 10 and 20 times the cylinder diameter in the longitudinal and transverse directions, respectively. Figure1 illustrates the computational domain employed in the present simulation with the boundary conditions. No-slip boundary conditions are imposed on the surface of the cylinder, and it has been chosen velocity inlet and pressure outlet for the inlet and outlet, respectively.

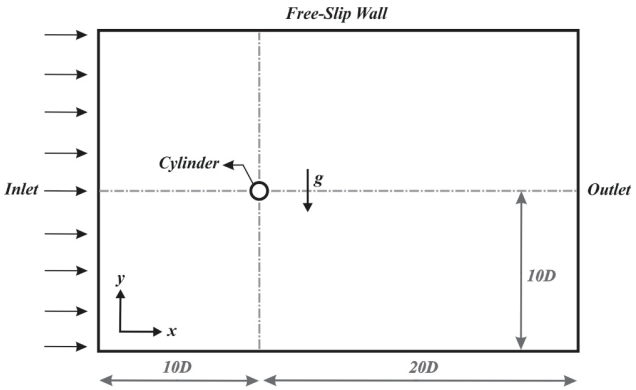

Figure 1. The computational domain around the circular cylinder.

Mesh Convergence

The computations are performed to study the grid independence for a non-buoyancy force (Ri=0) and stationary cylinder (Ω=0). The effect of the number of grids on the predicted average Nu and mean drag coefficient are shown in Table 1. It can be observed that an increase in grid nodes is accompanied by a decrease in the average Nu and mean drag coefficient. All models are implemented with a grid size of

Table 1. Influence of the grid size on the flow parameters for the circular cylinder at Re=40 and Ri=0

Mesh	Nods	Elements	$\underline{Nu}$	$\underline{C_D}$
12×17	2450	1980	3.320	1.647
24×34	9333	8880	3.295	1.619
48×68	36419	35520	3.291	1.619

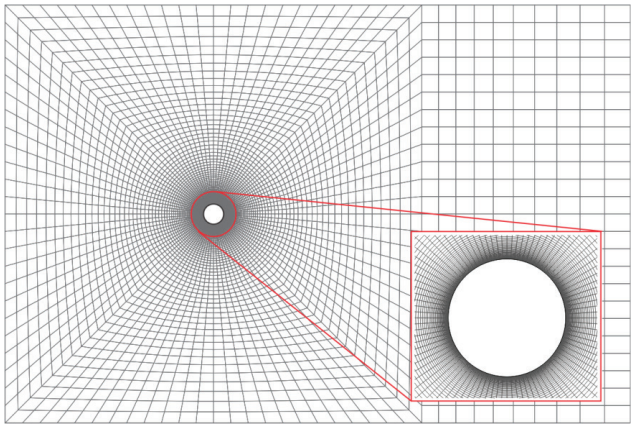

Figure 2. A grid used to compute the flow over the circular cylinder in this study (overview and close-up).

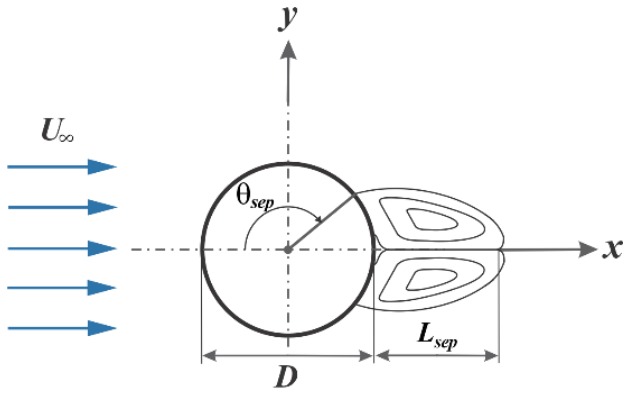

Figure 3. A Schematic and characteristics of the circular cylinder.

24×34 to save CPU time and maintain reasonable accuracy in the computations. Figure 2 shows the overview and a close-up of the selected grid of present work. Figure 3 illustrates the schematic and the characteristics of the circular cylinder.

Validation

The present simulations are compared with the available numerical and experimental data from the scientific literature. For numerical validation, the present results are compared with those of Biswas and Sarkar [3], Chatterjee and Sinha [6], Dennis et al. [17], Ding et al. [18], and Tuann and Olson [19]. Re 20 and 40 are chosen when there is no thermal buoyancy. A comparison between the present simulation and other studies is presented in Tables 2, 3, and 4 to verify the numerical accuracy. The results show acceptable agreement with experimental and numerical data for all Re. A comparison of the local Nu with Badr [20] and Biswas and Sarkar [3] is presented in Figure 4 to investigate the accuracy of the present numerical simulation. As can be seen, the results of the current work are reliable.

Table 2. A comparison of the average Nu for the flow over the circular cylinder for Re=20 and Re=40 at Ri=0 and Ω=0

Re	Author	$\underline{Nu}$
20	Biswas and Sarkar [3]	2.45
	Chatterjee and Sinha [6]	2.46
	Present Study	2.48
40	Biswas and Sarkar [3]	3.25
	Chatterjee and Sinha [6]	3.25
	Present Study	3.30

Table 3. A comparison of the mean drag coefficients, recirculation region, and separation angle for the flow over the circular cylinder for Re=20 and Re=40 at Ri=0 and Ω=0

Re	Author	$\underline{C_D}$	L_{sep}	θ_{sep}
20	Dennis et al. [16]	2.05	0.94	136.3
	Ding et al. [17]	2.18	0.93	135.9
	Tuann and Olson[18]	2.25	0.90	135.9
	Present Study	2.18	0.91	136.6
40	Dennis et al. [16]	1.52	2.35	126.2
	Ding et al. [17]	1.71	2.20	126.5
	Tuann and Olson [18]	1.67	2.10	125.2
	Present Study	1.62	2.14	126.3

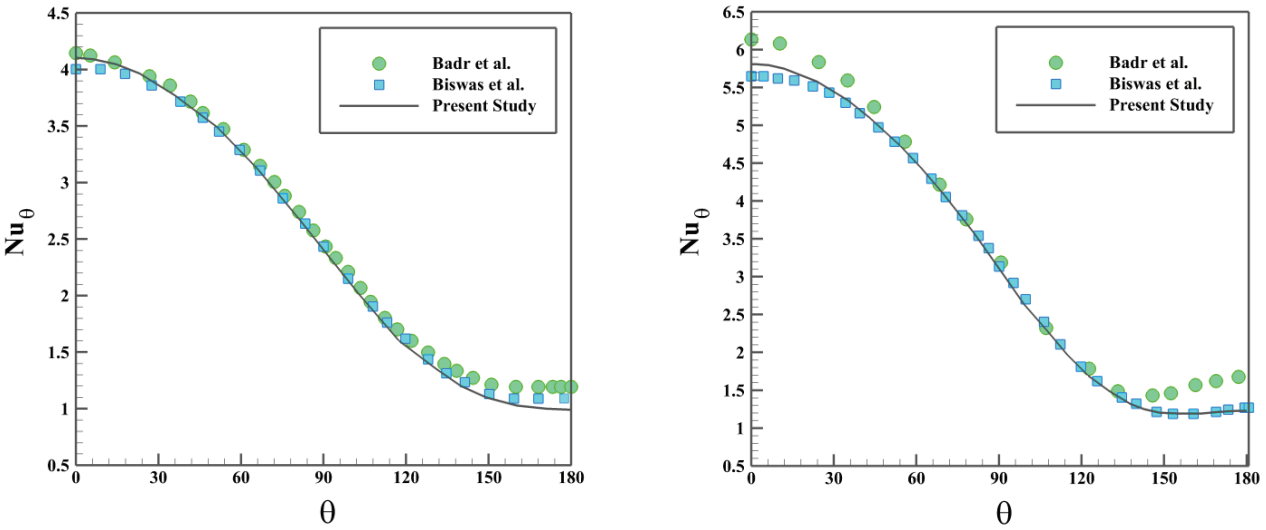

Figure 4. A comparison of the variation of the local Nu on the cylinder surface for (a) Re=20 and (b) Re=40 at Ri=0 and Ω=0 with Badr [19] and Biswas and Sarkar [3].

Table 4. Comparison of average Nu and St for flow over a circular cylinder at Re=100

Ri	Author	*Nu*	St
1	Chang et al. [21]	4.37	0.081
	Present Study	4.46	0.090

RESULTS AND DISCUSSION

The effect of the rotational direction and buoyancy force convection on aerodynamic and heat transfer parameters, including the lift coefficient, drag coefficient, and average and local Nu is considered. Figure 5 illustrates the lift coefficient as a function of Ri at different rotational speeds at Re 20 and 40. This Figure actually describes the net outcome of the interaction among the free stream, rotation-induced flow, and thermal buoyancy-induced flow. The results show that at a positive rotational speed (counterclockwise), an increase in Ri (in the direction of natural convection) is associated with an increase in the lift coefficient. At a negative rotational speed (clockwise), an increase in Ri is responsible for the decrease in the lift coefficient. The rotation of the cylinder leads to an increase in the absolute lift coefficient compared to the stationary cylinder at constant Ri. At positive rotation, the aerodynamic force is directed from top to bottom, and, consequently, the lift coefficient is negative. With the negative rotation, the aerodynamic force is from the bottom to top, and the lift coefficient is consequently positive.

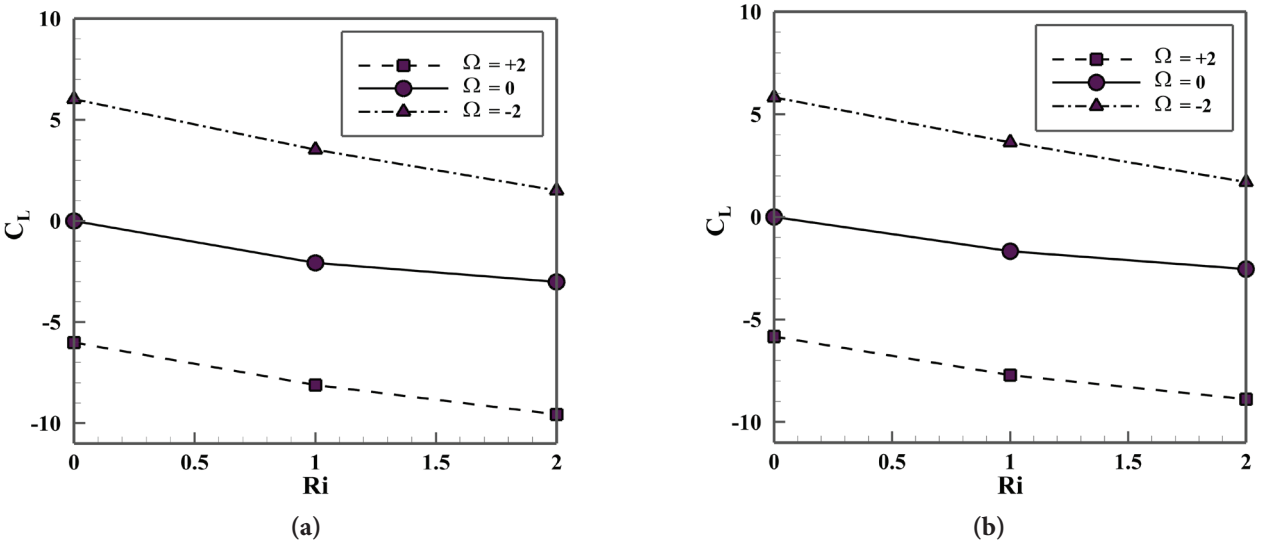

Figure 5. Variation of the lift coefficients against Ri at Pr=0.7 and different rotational speed (a) Re=20 (b) Re=40.

The drag coefficient as a function of Ri at different speeds is plotted at Pr of 0.7 and Re of 20 and 40, as shown in Figure 6. The drag coefficient decreases with an increase in Ri, except at the rotational speed of -2. For heated cylinders, the rotation of the cylinder in the positive direction also leads to a decrease in the mean drag coefficient. Furthermore, if we look at the streamline patterns in different Ri (not shown), we can see that heating causes the flow field to be closer to the surface of the cylinder and, consequently, the recirculation length of the vortices decreases, which eventually leads to a decrease in the average drag coefficient. Considering Figure 6, the drag coefficient is ordinarily positive for Ri <2, with increasing Ω at a constant Ri, it is established that the contribution of viscous drag increases and even becomes comparable with pressure drag at a larger rotational velocity. This phenomenon can be confirmed from the pressure variation along the cylinder surface where pressure at the front part of the cylinder decreases with increasing Ri whereas at rear part there is small increase in pressure.

To show the distribution of the average Nu around the heated cylinder, Figure 7 shows the rotation of the cylinder in both directions, which contributes to a decrease in the average Nu at all Ri. In addition, the counterclockwise

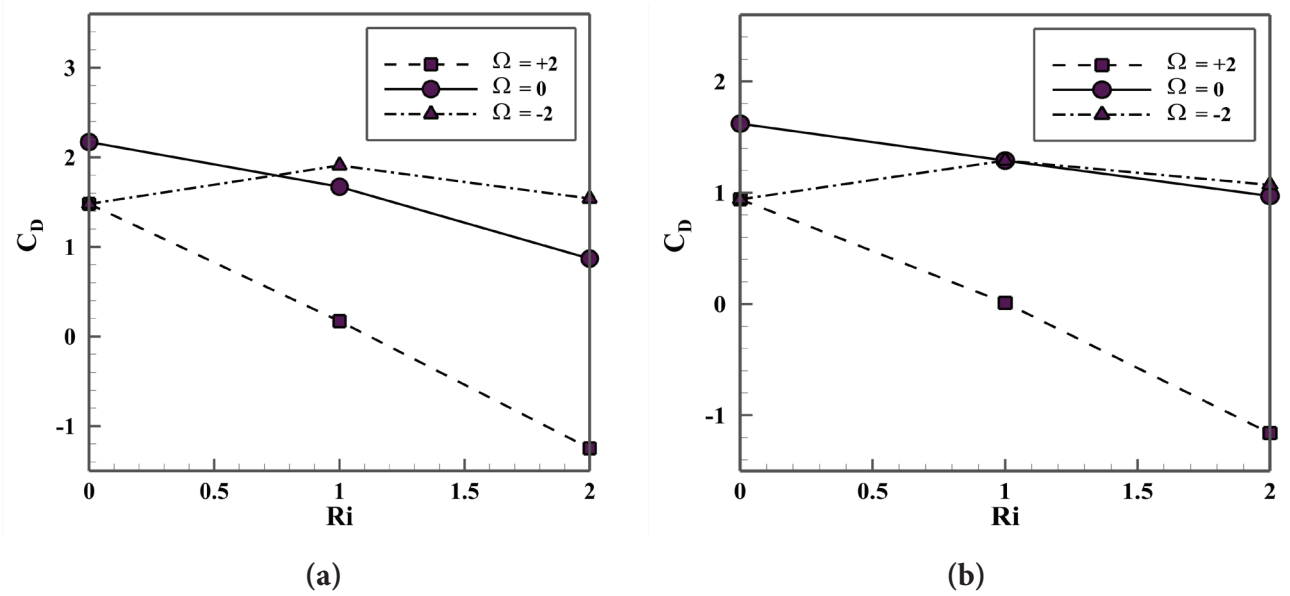

Figure 6. The variation of drag coefficients as a function of Ri at Pr=0.7 and different rotational speeds: (a) Re=20 (b) Re=40.

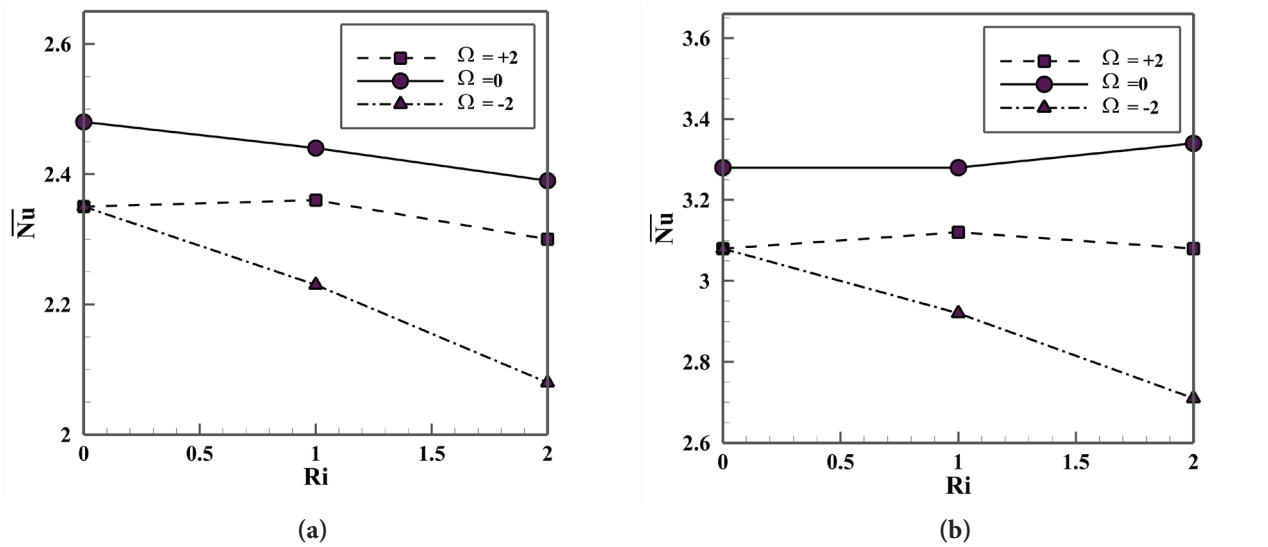

Figure 7. The variation of the average Nu as a function of Ri and different rotational speeds: (a) Re=20 (b) Re=40.

rotation of the cylinder may result in a higher average Nu at all Ri compared to the clockwise rotation. Competing effects of the thermal buoyancy and the positive rotation are found in Figure 7. The buoyancy attempts to make the flow unstable, whereas the positive rotation acts as a stabilizing agent. As a result of this competition, the flow which is naturally stable at the low Re becomes unstable with increasing buoyancy force. Conversely, the negative value of rotation fortifies the influence of buoyancy. This Figure shows that applying positive rotation can be considered an effective procedure for a drag reduction. Skin friction coefficient distribution over the surface of the cylinder is displayed in Figure8. In the event of the flow separation behind the cylinder, the skin friction decreases owing to having less surface area in contact with the fluid. In contrast, when the separation bubble is suppressed, the contact area with the fluid increases which gives rise to augmentation of the skin friction.

Employing Taguchi method helps us understand the importance of each variable for maximizing the Nu. This method treats variation as a factor of signal to noise ratio (SNR). Taguchi quality engineering method is utilized so as to study the influence of different parameters on heat transfer [22], more details can be found in Ref.[23] . In the present investigation important parameters, including the Re, Ri, and Ω, are considered. The larger the SNR is aimed, the more robust the outcome is against noise. Figure 9 shows controllable factors, indicating that the Re is more important than others in order to maximize Nu. The Nu and St are considered to be maximized (Large-Better) and minimized (Smaller-Better) [19]. By using the analysis of variance (ANOVA), the optimum combinations of the input parameters are more accurately determined, thereby providing the percent contribution of the input parameters on the sensitivity. The results of ANOVA analysis, R_Squared= 96.52 % confidence level, are presented in Table 5. From Figure 10 and Figure11, it can be found that higher amount of Nu is achievable as long as the rotation of cylinder is maintained at the positive low values. For example, when 30<Re<40, $|\Omega|$ should be less than 1 to experience higher Nu. It is interesting to see that the contours become asymmetric as Ri increases. Figure10 depicts that the effect of Re on Nu is more than Ω, substantiating Figure8. It is obvious that the difference between maximum and minimum values of the local Nu decreases with the increase in Re, regardless the direction and value of rotation. For the higher values of Re, this difference tends to vanish and local Nu number distribution on cylinder circumference inclines to be straight line.

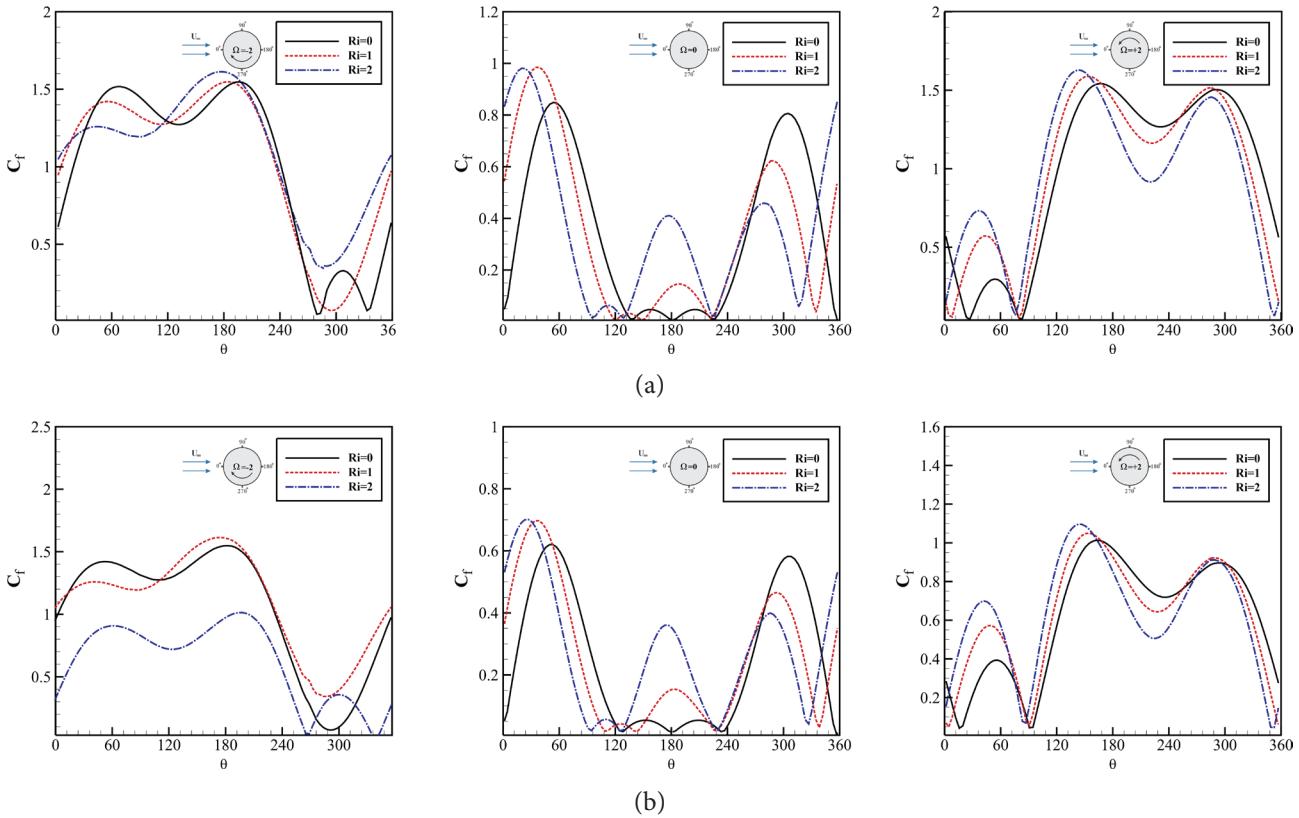

Figure 8. Skin friction coefficient distribution over the surface of the cylinder for different rotational speeds: (a) Re=20 (b) Re=40.

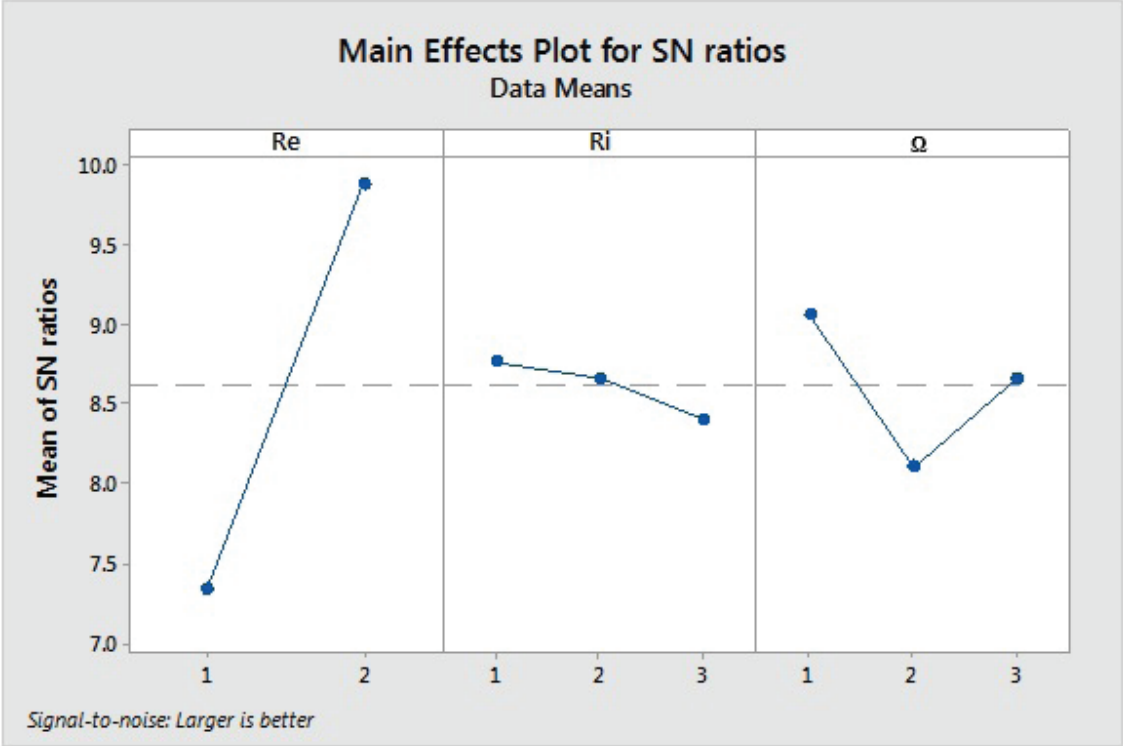

Figure 9. Signal-to-noise ratios for Nu.

Table 5. Analysis of Variance for the Nu number

Source	DF	Sum of square	Mean of square	F-Value	P-Value
Re	1	2.8322	2.8322	300.62	0
Ri	2	0.03548	0.01774	1.88	0.194
Rot.	2	0.27218	0.13609	14.44	0.001
Error	12	0.11306	0.00942		
Total	17	3.25291			

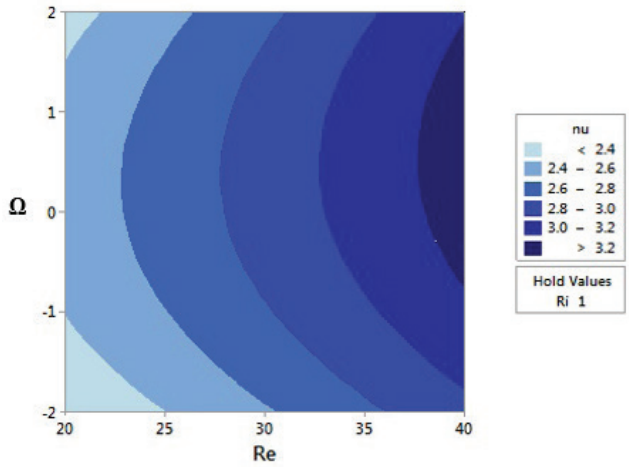

Figure 10. The contour of the Nu as a function of Re and Ω.

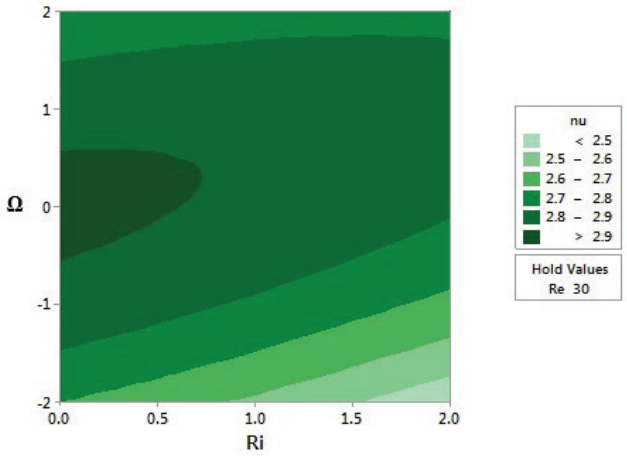

Figure 11. The contour of the Nu as a function of Ri and Ω.

The distribution of the local Nu around the heated cylinder is also computed for Re of 20 and 40 in Figs. 12 and 13, respectively. The results suggest that in the stationary cylinder (Ω=0), the maximum local Nu is located at the stagnation point (θ=180°). With an increase in Ri, the maximum local Nu is slightly pulled up, and the angle becomes smaller. It bears noting that the local Nu in the stationary cylinder increases significantly in the upper half of the cylinder (0<θ< 180) compared to its lower half (180<θ< 360). This is because the interaction of the thermal buoyancy flow and fluid flow can increase the thickness of the thermal layer in the lower half and thus a decrease in the local Nu. Looking at the backside of a cylinder, we find that as Ri increases, so does the local Nu. This is mainly down to the fact that the superimposed thermal buoyancy force leads to an increase in the adhesion boundary layer on the cylinder surface, which increases the local Nu. It is also worth noting that the rotation of the cylinder causes a change in the distribution of the local Nu. The extreme points of the local Nu depend on the rotational direction of the cylinder. When the rotational direction is positive, the maximum local Nu shifts down to θ=225°, and the minimum local Nu shifts up to θ=100°. When the rotational direction is negative, the maximum local Nu shifts up to θ=140°, and the minimum local Nu shifts down to θ=270°. This is because in a rotating cylinder, the fluid particles always move in opposite directions in the upper and lower parts due to the shear stress on the cylinder surface when the flow is free. In rotational directions, the particle motions on the top of the cylinder are opposite to the fluid flow, while the particle motions on the bottom coincide with the fluid flow. This increases the boundary layer thickness on the top side and, consequently, a decrease in the local Nu (vortices formed on top of the cylinder). Also, in the lower half of the cylinder, the thickness of the boundary layer on the bottom side decreases, and consequently, the local Nu increases.

St for Re of 20 and 40 and different Ri and rotational speeds are presented in Table 6. As can be seen, St increases with an increase in Ri. In fact, the superimposed thermal buoyancy force causes an unstable fluid flow regime and induces VS over the cylinder. The rotational direction can also have a significant effect on VS and St. Using Taguchi

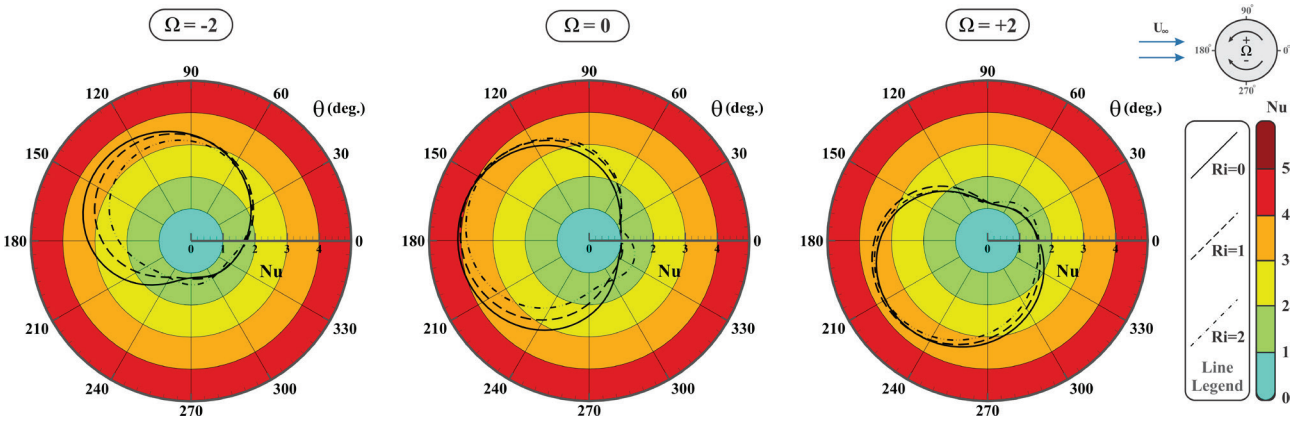

Figure 12. The variation of the local Nu along the cylinder at different Ri and rotational speeds at Re=20 and Pr=0.7.

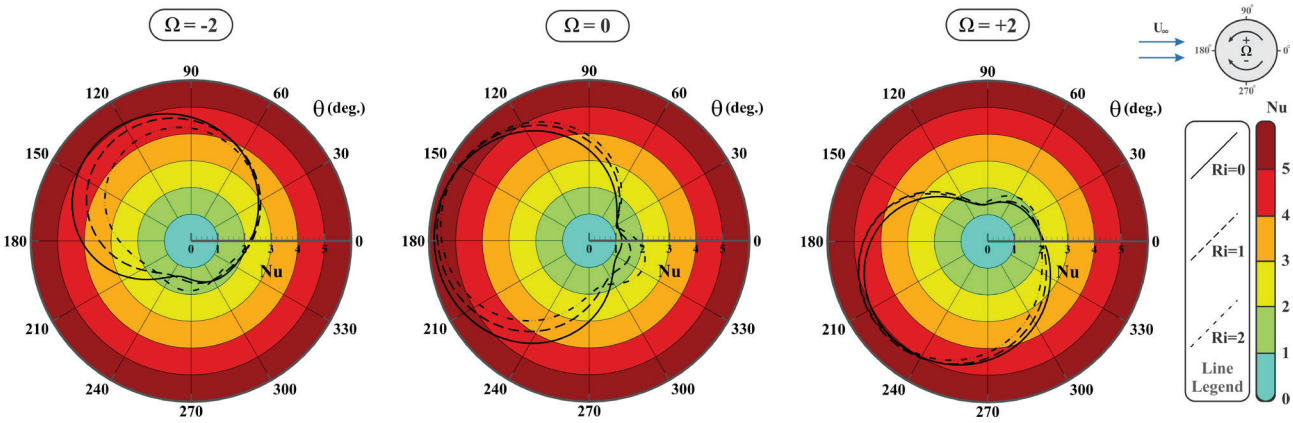

Figure 13. Distribution of the local Nu along the cylinder in different Ri and rotational speeds at Re=40 and Pr=0.7.

Table 6. A comparison of St for Re=20 and Re=40 at different rotational speeds, Ri, and Pr=0.7

Re	Ω	Ri	Regime	St
20	-2	0	Steady	0
		1	Steady	0
		2	Transient	0.051
	0	0	Steady	0
		1	Steady	0
		2	Transient	0.055
	2	0	Steady	0
		1	Steady	0
		2	Transient	0.63
40	-2	0	Steady	0
		1	Steady	0
		2	Steady	0
	0	0	Steady	0
		1	Transient	0.121
		2	Transient	0.131
	2	0	Steady	0
		1	Steady	0
		2	Transient	0.093

as a powerful tool for performance optimization, and considering the lowest St can result in Signal-to-noise ratios for St (Figure14). This Figure shows SNR criterion for controllable factors, indicating that the rotation of cylinder is of paramount to stabilize the flow patterns, thereby making the effect of other parameters to be less visible. It is worth mentioning that Chatterjee and Sinha [24] found that St is influenced by two competing physical phenomenon, one is the heating that gives rise to the boundary layer along the cylinder surface to be accelerated resulting in a subsequent enhancement of the shedding frequency, and the other is the rotation that acts as a stabilizing agent resulting in the decrease of shedding frequency. This study substantiates their findings, and shows that rotation is deciding factor.

At Re=20, a negative rotational direction decreases St compared with the stationary cylinder; and a positive rotational speed increases it. But at Re=40, the rotation of the cylinder in either direction results in a decrease in St. The time history of the average Nu and lift coefficients is shown in Figure 15 for a full period. As shown, the variations of the lift coefficient and the average Nu are negligible, so the use of the average value is appropriate.

Contour plots of x-velocity are shown in Figures 16 and 17 for Re of 20 and 40, respectively. For cases with the VS

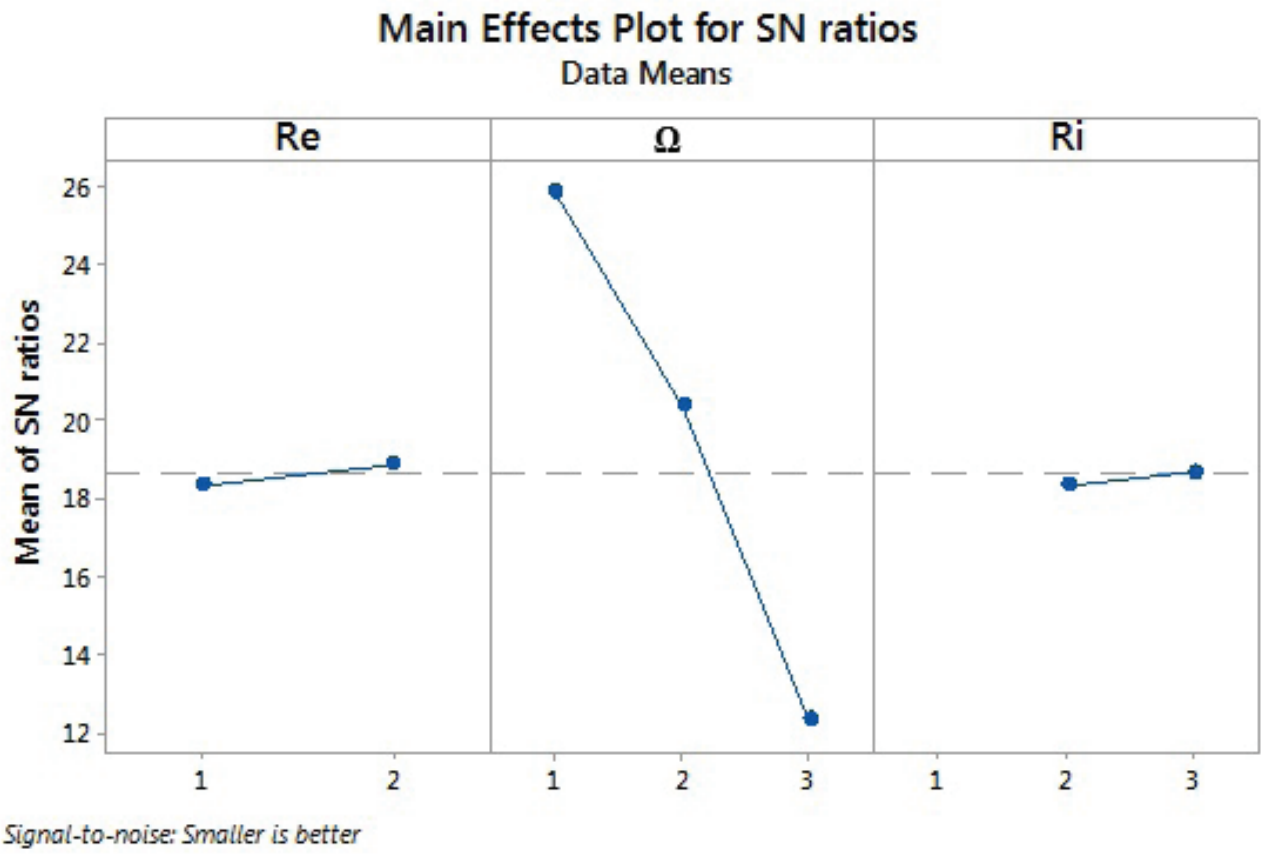

Figure 14. Signal-to-noise ratios for St.

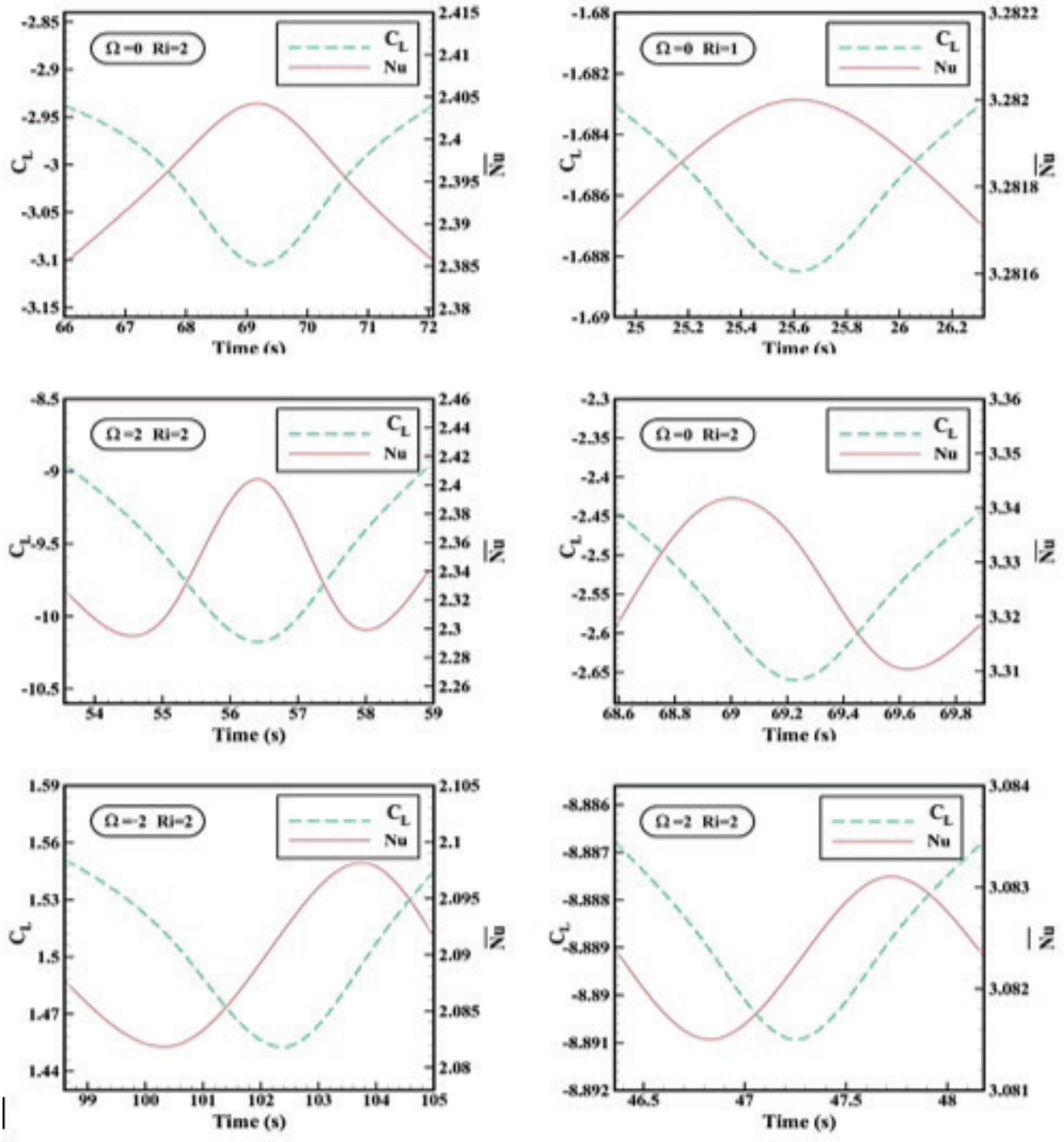

Figure 15. The variation of the lift coefficients and average Nu for one period at (a) Re=20 and (b) Re=40 in transient cases and Pr=0.7.

phenomenon, VS is shown on the corresponding contour. The rotation of the cylinder at constant Ri also leads to a disruption of the symmetry of the air velocity contours. At positive rotational speeds, the shear stress caused by the rotation of the cylinder drives the motion of the air below the cylinder faster, and the friction slows down the fluid motion on the top of the cylinder.

Physically, as the rotational speed increases, a greater volume of fluid rotates with the cylinder regardless of the direction of rotation. Therefore, the pressure distribution will create a force. Also, the heating increases the velocity in the wake region, causing the shear layer and the roll-up process. When Ri increases, the consequence of thermal buoyancy becomes more prominent, and the fluid certainly flows upward in the wake region of the cylinder. Accordingly, the incoming air below the cylinder accelerates as the principle of mass conservation is satisfied. As a result, the mass flow below the cylinder becomes larger than that

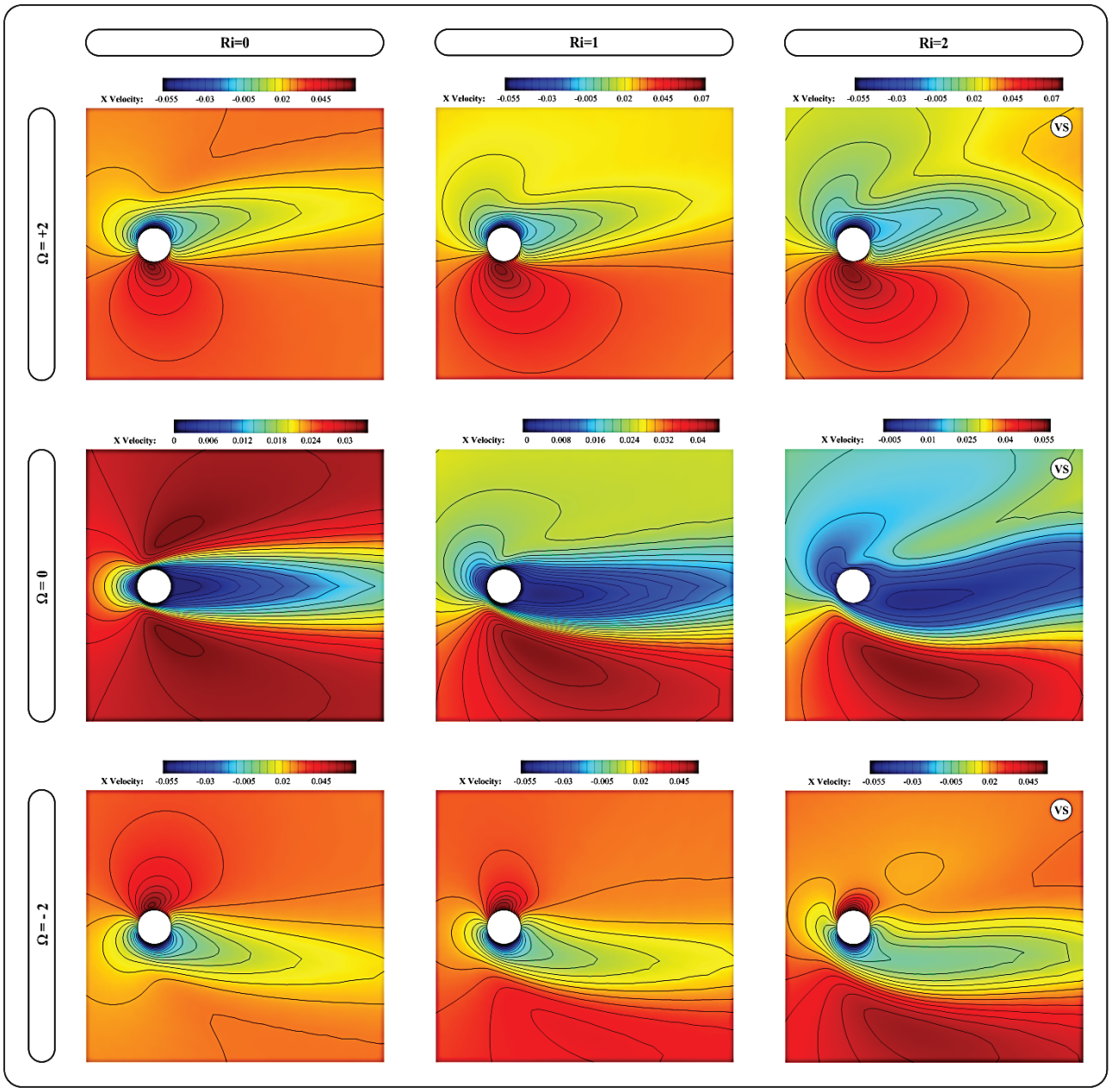

Figure 16. Velocity contour for different rotational speeds and Ri at Pr=0.7 and Re=20.

above the cylinder, and the resulting flow structure tends to become asymmetric. This translates into experiencing the negative lift coefficient. Also at negative rotational speeds, the velocity at the top of the cylinder is greater than that at the bottom. Consequently, the pressure and lift coefficients are positive from the bottom to the top of the cylinder (the lift coefficient is positive).

The isotherm contour plots are shown in Figs. 18 and 19 for Re of 20 and 40, respectively. The thermal boundary layer is symmetrical in the stationary cylinder for Re of 20 and 40. The thickness of the thermal boundary layer increases with an increase in Ri, and consequently, the average Nu decreases. When the cylinder rotates, the distribution of thermal boundary layer thickness becomes asymmetric, and the local Nu floats around the cylinder. The boundary layer is thinner at positive rotational speed than at negative rotational speed due to the interaction between gravity and rotational direction, so the heat transfer in the positive rotational direction is higher than in the negative one. It is clear that buoyancy is partly responsible for the asymmetry of the isothermal contours, and a combination of rotation and buoyancy leads to the formation of the region where there is a high temperature adjacent to the cylinder. The inclusion of the buoyancy force in the stationary cylinder leads to a partial enlargement of the boundary layer and vortex shedding.

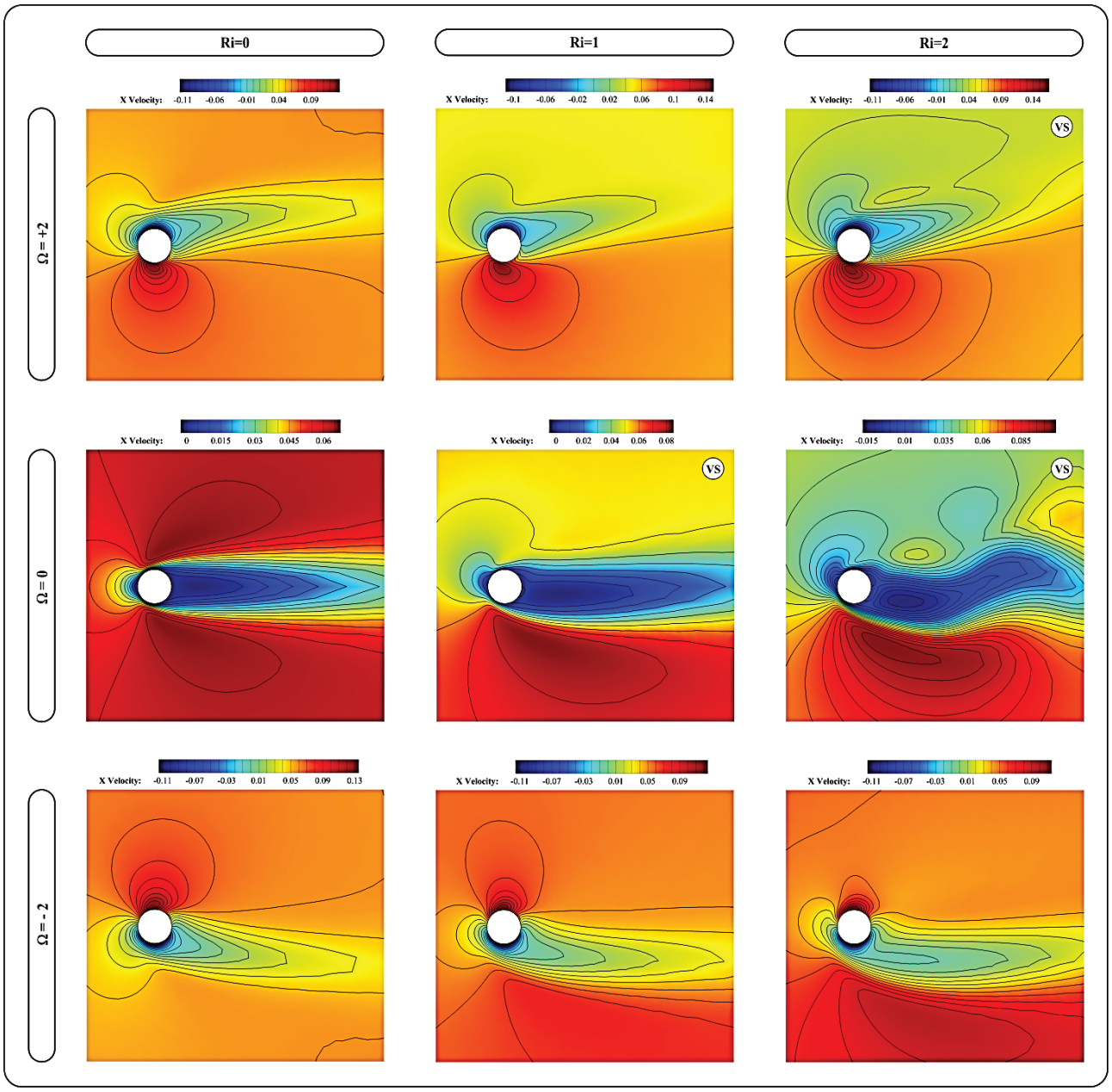

Figure 17. Velocity contour for different rotational speeds and Ri at Pr=0.7 and Re=40.

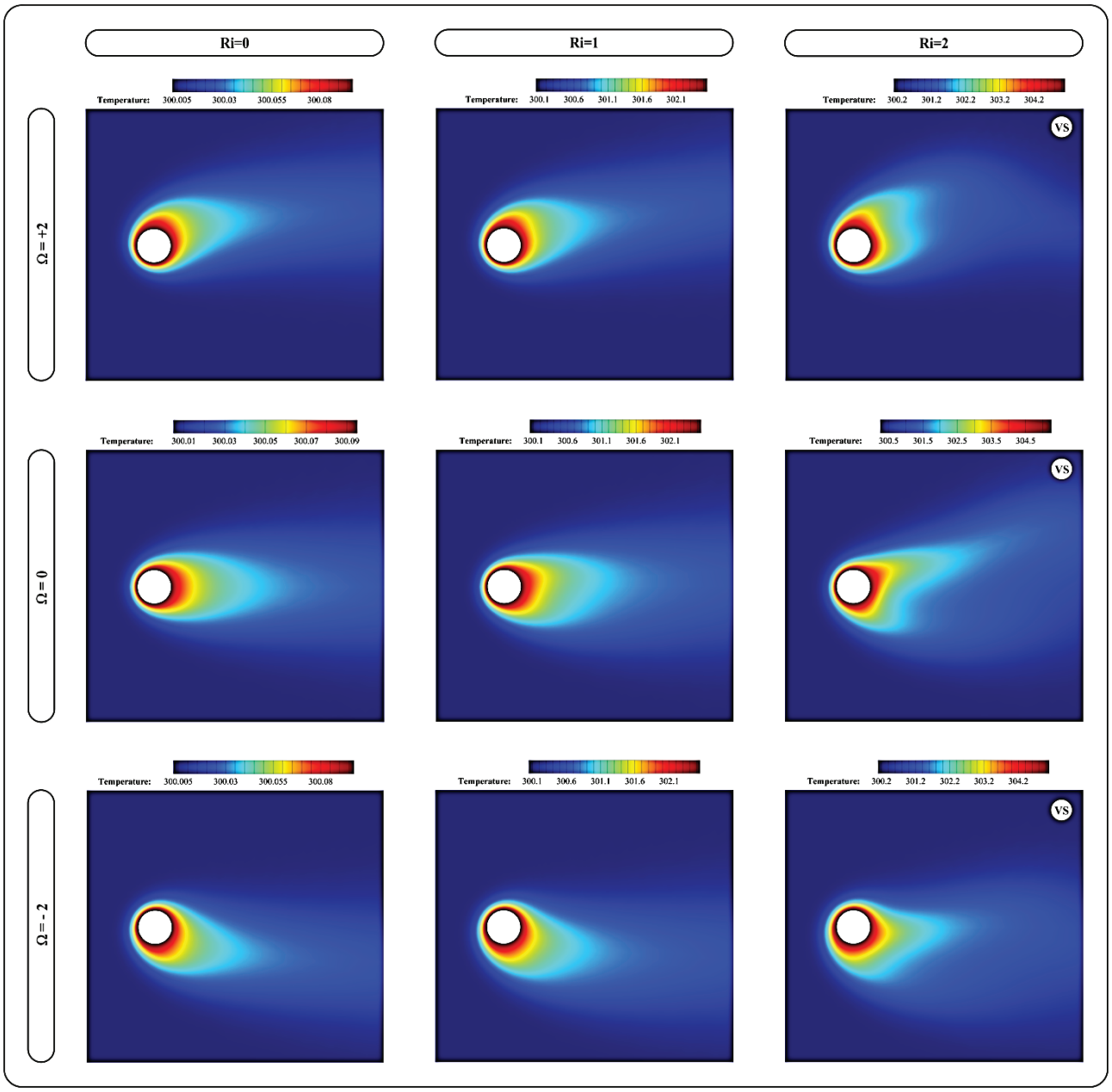

Figure 18. Temperature contour for different rotational speeds and Ri at Pr=0.7 and Re=20.

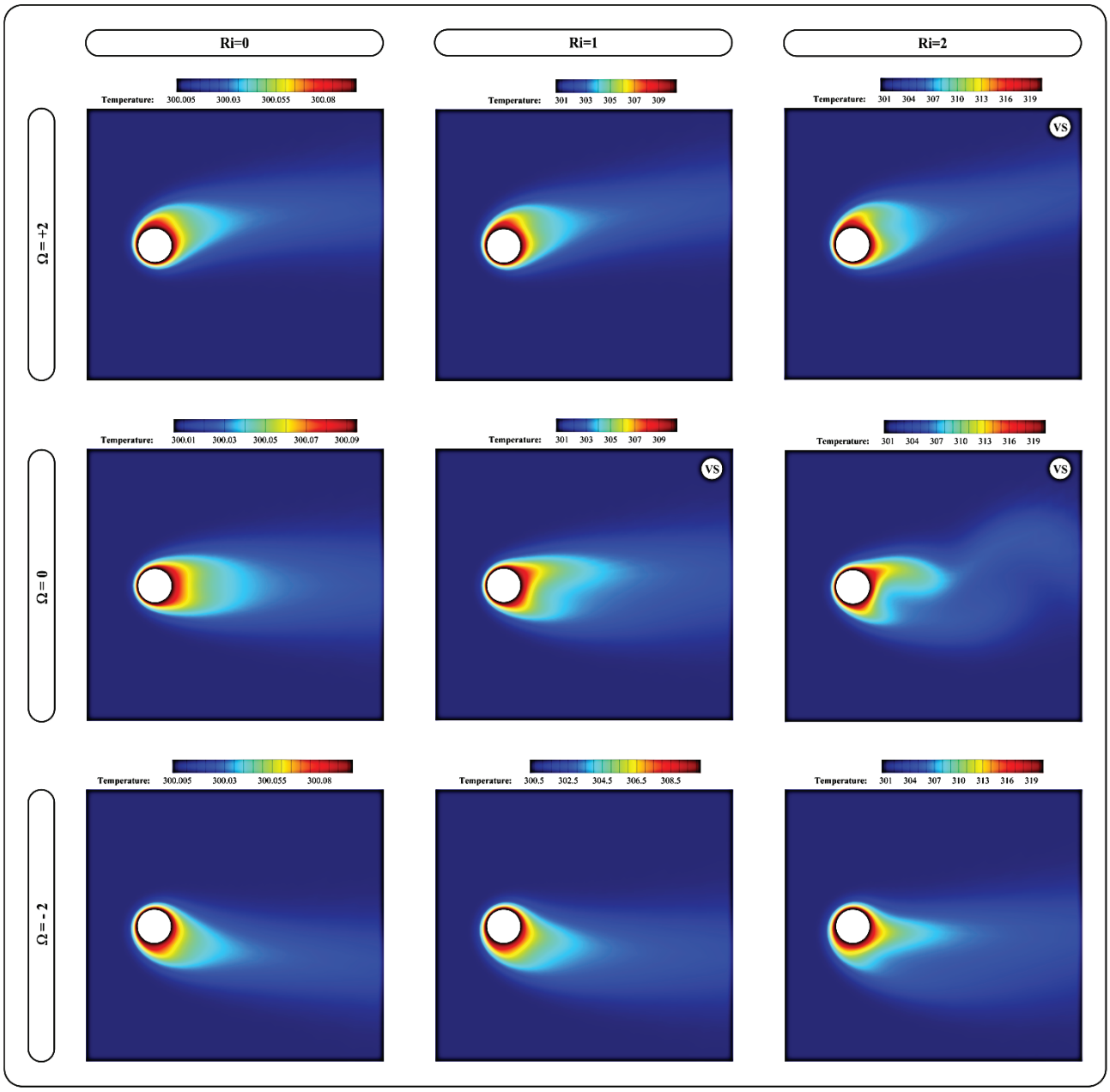

Figure 19. Temperature contour for different rotational speeds and Ri at Pr=0.7 and Re=40.

CONCLUSIONS

For the numerical simulation, a laminar incompressible flow of a Newtonian fluid with constant thermophysical properties is assumed together with the Boussinesq approximation. The flow field and heat transfer near the rotating cylinder are numerically simulated under the influence of VS. The main starting point of this study is to understand the interaction between buoyancy and rotation. The main results of this study can be outlined as follows:

1) At positive rotational speed, an increase in Ri leads to an increase in the lift coefficient, and at negative rotational speed, an increase in Ri is responsible for the decrease in the lift coefficient.

2) The drag coefficient decreases with an increase in Ri except at a rotational speed of 0. Also, for heated cylinders, rotation of the cylinder in the positive direction decreases the average drag coefficient.

3) Rotation of the cylinder in the positive direction has a higher average Nu in each Ri in relation to the negative direction.

4) VS and the Strouhal number can be significantly affected by the direction of rotation.

The results attained by the Taguchi method realized that the efficiency of Reynolds number parameter on the Nusselt number and the rotation of cylinder on Strouhal number are too much in comparison with other metrics, and so other parameters are of little consequence.

NOMENCLATURE

C_D	Drag Coefficient
C_L	Lift Coefficient
D	Cylinder diameter, m
g	Acceleration, m/s^2
h	Local heat transfer coefficient, W/m^2.K
k	thermal conductivity of fluid, W/m.K
L_s	Eddy length, m
L_{sep}	Non-dimensional eddy length
$\underline{Nu}$	Average Nusselt number over the cylinder surface
P	Pressure, N/m^2
Pr	Prandtl number
Re	Reynolds number
Ri	Richardson number
St	Strouhal number
t	Time, t
T	Temperature, K
u, v	dimensionaless velocity components in x and y directions, m/s
U_∞	Freestream Velocity, m/s
x, y	dimensionless coordinates, m

Greek symbols

α	Thermal diffusivity of a fluid, m^2/s
β	Thermal expansion coefficient, 1/K
μ	Viscosity of a fluid, N.s/m^2
ρ	Density of a fluid,kg/m^3
Θ	Non-dimensional temperature
ν	Kinematic viscosity of the fluid, m^2/s
θ	Angular location on the cylinder surface from the leading point,°
θ_{sep}	Separation angle,°
ω	Rotation Speed,rev/s
Ω	Non-dimensional rotation Speed

Subscript

∞	Free stream condition
w	Wall

AUTHORSHIP CONTRIBUTIONS

Authors equally contributed to this work.

DATA AVAILABILITY STATEMENT

The authors confirm that the data that supports the findings of this study are available within the article. Raw data that support the finding of this study are available from the corresponding author, upon reasonable request.

CONFLICT OF INTEREST

The author declared no potential conflicts of interest with respect to the research, authorship, and/or publication of this article.

ETHICS

There are no ethical issues with the publication of this manuscript.

REFERENCES

[1] Jain PC, Lohar BL. Unsteady mixed convection heat transfer from a horizontal circular cylinder. J Heat Transf 1979;101:126−131. [CrossRef]

[2] Yang H, Zhang W, Zhu Z. Unsteady mixed convection in a square enclosure with an inner cylinder rotating in a bi-directional and time-periodic mode. Int J Heat Mass Transf 2019;136:563−580. [CrossRef]

[3] Biswas, G. and S. Sarkar. Effect of thermal buoyancy on vortex shedding past a circular cylinder in cross-flow at low Reynolds numbers. Int J Heat Mass Transf 2009;52:1897−1912. [CrossRef]

[4] Paramane, S.B. and A. Sharma. Effect of cross-stream buoyancy and rotation on the free-stream flow and heat transfer across a cylinder. International J Thermal Sci 2010;49:2008−2025. [CrossRef]

[5] Al-Sumaily GF, Dhahad HA, Hussen HM, Thompson MC. Influence of thermal buoyancy on vortex shedding behind a circular cylinder in parallel flow. Int J Therm Sci 2020;156:106434. [CrossRef]

[6] Chatterjee D, Sinha C. Influence of thermal buoyancy on vortex shedding behind a rotating circular cylinder in cross flow at subcritical Reynolds numbers. J Heat Transf 2014;136:051704. [CrossRef]
[7] Nguyen, HD, Paik S, Douglass R. Unsteady mixed convection about a rotating circular cylinder with small fluctuations in the free-stream velocity. Int J Heat Mass Transf 1996;39:511−525. [CrossRef]
[8] Elghnam RI. Experimental and numerical investigation of heat transfer from a heated horizontal cylinder rotating in still air around its axis. Ain Shams Eng J 2014;5:177−185. [CrossRef]
[9] Luo X, Zhang W, Dong H, Kumar Thakur A, Yang B, Zhao W. Numerical analysis of heat transfer enhancement of fluid past an oscillating circular cylinder in laminar flow regime. Prog Nucl Energy 2021;139:103853. [CrossRef]
[10] Wan H, DesRoches JA, Palazotto AN, Patnaik SS. Vortex-induced vibration of elliptic cylinders and the suppression using mixed-convection. J Fluids Struct 2021;103:103297. [CrossRef]
[11] Mahir N, Altaç Z. Numerical investigation of flow and combined natural-forced convection from an isothermal square cylinder in cross flow. Int J Heat Fluid Flow 2019;75:103−121. [CrossRef]
[12] Rashidi MM, Sadri M, Sheremet MA. Numerical simulation of hybrid nanofluid mixed convection in a lid-driven square cavity with magnetic field using high-order compact scheme. Nanomaterials 2021;11:2250. [CrossRef]
[13] Erfani E, Rashidi MM Parsa AB. The modified differential transform method for solving off-centered stagnation flow toward a rotating disc. Int J Comput Methods 2010;7:655−670. [CrossRef]
[14] Barati E, Biabani M, Zarkak MR. Numerical investigation on vortex-induced vibration energy harvesting of a heated circular cylinder with various cross-sections. Int Commun Heat Mass Transf 2022;132:105888. [CrossRef]
[15] Hussain S, Jain J, Seth G, Rashidi M. Free convective heat transfer with hall effects, heat absorption and chemical reaction over an accelerated moving plate in a rotating system. J Magn Magn Mater 2017;422:112−123. [CrossRef]
[16] ANSYS Inc. ANSYS Fluent Theory Guide. 14.0 Theory Guide. Pennsylvania, USA: ANSYS INC; 2011, p. 218−221.
[17] Dennis SCR, Hudson J, Smith N. Steady laminar forced convection from a circular cylinder at low Reynolds numbers. Phys Fluids 1968;11:933−940. [CrossRef]
[18] Ding H, Shu C, Yeo K, Xu D. Simulation of incompressible viscous flows past a circular cylinder by hybrid FD scheme and meshless least square-based finite difference method. Comput Methods Appl Mech Eng 2004;193:727−744. [CrossRef]
[19] Tuann S-Y, Olson MD. Numerical studies of the flow around a circular cylinder by a finite element method. Comput Fluids 1978;6:219−240. [CrossRef]
[20] Badr H. Laminar combined convection from a horizontal cylinder-parallel and contra flow regimes. Int J Heat Mass Transf 1984;27:15−27. [CrossRef]
[21] Chang, K.-S. and J.-Y. Sa. The effect of buoyancy on vortex shedding in the near wake of a circular cylinder. J Fluid Mech1990;220:253−266. [CrossRef]
[22] Javadpour SM, Abadi EAJ, Akbari OA, Goharimanesh M. Optimization of geometry and nano-fluid properties on microchannel performance using Taguchi method and genetic algorithm. International Commun Heat Mass Transf 2020;119:104952. [CrossRef]
[23] Ruefer H. Living without Mathematical Statistics: Accurate Analysis, Diagnosis, and Prognosis Based on the Taguchi Method. New York: Springer; 2018. [CrossRef]
[24] Chatterjee D, Sinha C. Effect of Prandtl number and rotation on vortex shedding behind a circular cylinder subjected to cross buoyancy at subcritical Reynolds number. Int Commun Heat Mass Transf 2016;70:1-8. [CrossRef]